Interfacial Debonding Analysis in Nanoparticulate Reinforced Metal Matrix Composites of AA8090/Zirconium Carbide

[1]B. Kotiveera Chari and A. Chennakesava Reddy

[1]Professor, Department of Mechanical Engineering, NIT, Warangal, India
[2]Assistant Professor, Department of Mechanical Engineering, MJ College of Engineering and Technology, Hyderabad, India
dr_acreddy@yahoo.com

Abstract: A hexagonal array unit cell/2-D rectangular particulate RVE models were employed to assess interfacial debonding using cohesive zone analysis. The particulate metal matrix composites are zirconium carbide/AA8090 alloy at different volume fractions of zirconium carbide. Interface debonding was observed in all the composites. The strain energy density has increased with ease of interfacial debonding.

Keywords: AA8090, zirconium carbide, rectangular particulate, RVE model, finite element analysis, interface debonding.

1. INTRODUCTION

The relation between ply uniaxial strengths and constituent properties of structure is obtained through the composite micromechanics. An external load applied to a composite is partly borne by the matrix and partly by the reinforcement. The load carried by the matrix across a section of the composite is given by the product of the average stress in the matrix and its sectional area. The load carried by the reinforcement is determined similarly. In studying the interfacial bonding behavior of composites under tensile stress, Cox [1] and Piggott [2] derived the interfacial shear strength as a function of tensile strain of matrix and composite, elastic modulus of fiber, aspect ratio of fiber and distance from center to end of fiber. Nan and Clarke [3] analyzed the mechanical properties of the particle reinforced composites using the dislocation theory from the materials sciences point of view. Micromechanics are adopted for 10%, 20% and 30% of the volume fraction of particle and for several particle shapes through finite element simulation by using unit cell models [4-17].

In the present research, interfacial debonding analysis was carried out using cohesive zone models in AA8090/zirconium carbide nanoparticulate-reinforced metal matrix composites. Representative volume elements (RVEs) models were taken from the periodic 2-D rectangular particulates in a hexagonal array distribution.

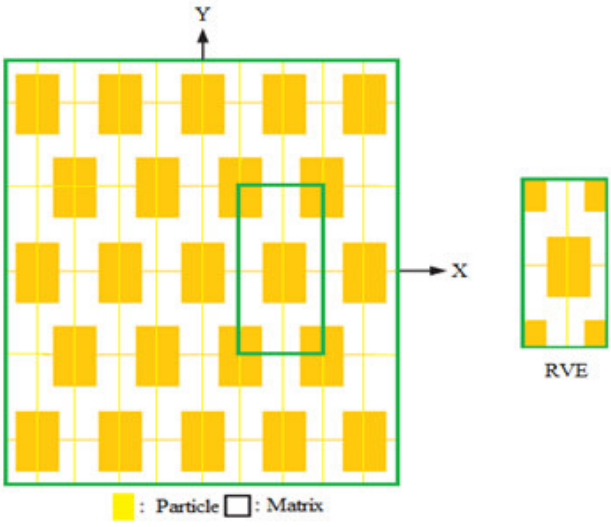

Figure 1: The RVE model.

2. MATERIALS AND METHODS

The volume fractions of zirconium carbide used in the present work were 10%, 20%, and 30%. The matrix material was AA8090 alloy. The periodic model for the representative volume element (RVE) scheme was constructed from 2-D rectangular

particulates in a hexagonal array particulate distribution (figure 1). PLANE183 element was used for the matrix and the nanoparticulates. The cohesive zone can be incorporated in the continuum formulation by applying the cohesive tractions as boundary conditions. The cohesive element is implemented as a linear element with four nodes. The iso-parametric formulation is chosen for the element, meaning that shape and displacements are interpolated by the same shape functions.

Shear-log model is based on the assumption that all of the load transfer from matrix to particulate occurs via shear stresses acting on the particulate interface between the two constituents. The rate of change of the stress in the particulate to the interfacial shear stress at that point and the particulate radius, 'r' is given by:

$$\frac{d\sigma_p}{dx} = -\frac{2\tau_i}{r} \quad (1)$$

which may be regarded as the basic shear lag relationship.

The stress distribution in the particulate is determined by relating shear strains in the matrix around the particulate to the macroscopic strain of the composite. Some mathematical manipulation leads to a solution for the distribution of stress at a distance 'x' from the mid-point of the particulate which involves hyperbolic trig functions:

$$\sigma_p = E_p\varepsilon_c[1 - cosh(nx/r)sech(ns)] \quad (2)$$

where ε_c is the composite strain, s is the particulate aspect ratio (length/diameter) and n is a dimensionless constant given by:

$$n = \left[\frac{2E_m}{E_p(1+v_m)ln(1+v_p)}\right]^{1/2} \quad (3)$$

in which v_m is the Poisson ratio of the matrix. The variation of interfacial shear stress along the particulate length is derived, according to Equation (1), by differentiating this equation, to give:

$$\tau_i = \frac{n\varepsilon_c}{2}E_p sinh\left(\frac{nx}{r}\right)sech(ns) \quad (4)$$

The equation for the stress in the particulate, together with the assumption of a average tensile strain in the matrix equal to that imposed on the composite, can be used to evaluate the composite stiffness. This leads to:

$$\sigma_c = \varepsilon_c\left[v_pE_p\left(1 - \frac{tanh(ns)}{ns}\right) + (1 - v_p)E_m\right] \quad (5)$$

The expression in square brackets is the composite stiffness. The stiffness is a function of particulate aspect ratio, particulate/matrix stiffness ratio and particulate volume fraction.

If the particle deforms in an elastic manner (according to Hooke's law) then,

$$\tau = \frac{n}{2}\sigma_p \quad (6)$$

If particle fracture occurs when the stress in the particulate reaches its ultimate tensile strength, $\sigma_{p,uts}$, then setting the boundary condition at

$$\sigma_p = \sigma_{p,\,uts} \quad (7)$$

and substituting into Equation (6) gives a relationship between the strength of the particle and the interfacial shear stress such that if

$$\sigma_{P,uts} < \frac{2\tau}{n} \quad (8)$$

Then the particle will fracture. Similarly if interfacial debonding/yielding is considered to occur when the interfacial shear stress reaches its shear strength

$$\tau = \tau_{max} \quad (9)$$

For particle/matrix interfacial fracture can be established whereby,

$$\tau_{max} < \frac{n\sigma_p}{2} \quad (10)$$

This approach suggests that the outcome of a matrix crack impinging on an embedded particle depends on the balance between the particle strength and the shear strength of the interface.

For plane strain conditions, the macro stress- macro strain relation is as follows:

$$\begin{Bmatrix}\overline{\sigma_x}\\ \overline{\sigma_y}\\ \overline{\tau_{xy}}\end{Bmatrix} = \begin{bmatrix}\overline{C_{11}} & \overline{C_{12}} & 0\\ \overline{C_{21}} & \overline{C_{22}} & 0\\ 0 & 0 & \overline{C_{33}}\end{bmatrix} \times \begin{Bmatrix}\overline{\varepsilon_x}\\ \overline{\varepsilon_y}\\ \overline{\gamma_{xy}}\end{Bmatrix} \quad (11)$$

The interfacial tractions can be obtained by transforming the micro stresses at the interface as given in Eq. (3):

$$t = \begin{Bmatrix}t_z\\ t_n\\ t_t\end{Bmatrix} = T\sigma \quad (12)$$

$$\text{where, } T = \begin{bmatrix} 0 & 0 & 0 \\ cos^2\theta & sin^2\theta & 2sin\theta cos\theta \\ -sin\theta cos\theta & sin\theta cos\theta & cos^2\theta - sin^2\theta \end{bmatrix}$$

3. RESULTS AND DISCUSSION

The tensile modulus increased with volume fraction of zirconium carbide as shown figure 2a. Compression modulus is, respectively, 159.96 GPa, 152.23 GPa and 158.03 GPa of AA8090/10%ZrC, AA8090/20%ZrC and AA8090/30%ZrC composites. The shear modulus decreased with increase in the volume fraction of ZrC in the composites (figure 2b). The major Poisson's ratios are, respectively, 0.52, 0.52 and 0.51 for AA8090/10%ZrC, AA8090/20%ZrC and AA8090/30%ZrC composites (figure 2c). The difference in the elastic moduli of ZrC particulates and AA8090 alloy matrix is 353 GPa. The Poisson's ratios of AA8090 alloy matrix and ZrC particulates are, respectively, 0.33 and 0.25.

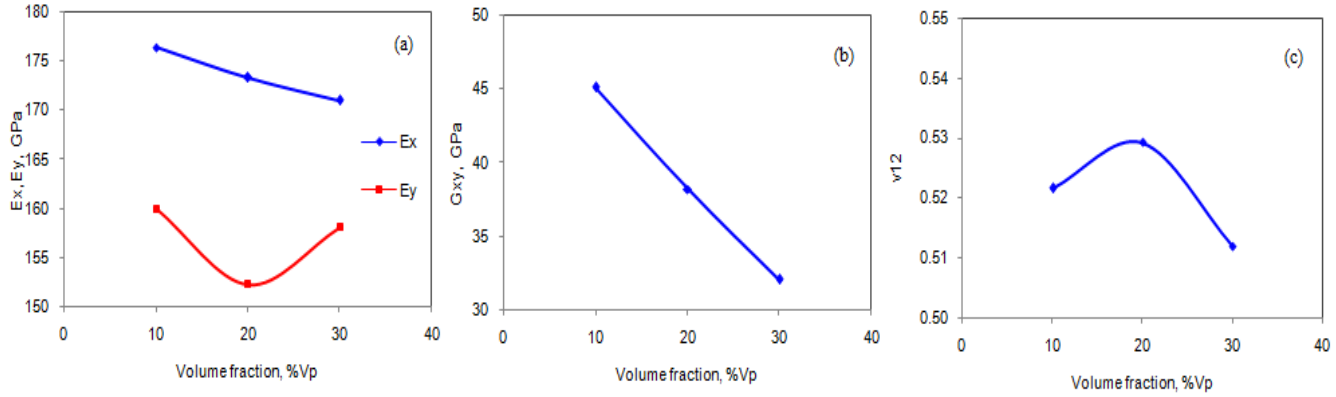

Figure 2: Effect of volume fraction on effective material properties.

The condition $\tau_{max} < n\sigma_p/2$ satisfied for the occurrence of debonding in the composites including 10%, 20% and 30% ZrC (figure 4b). The ZrC particulate fracture was not found in the AA8090/ZrC composites as shown in figure 3b as the condition $\sigma_p \leq 2\tau/n$ did not satisfied.

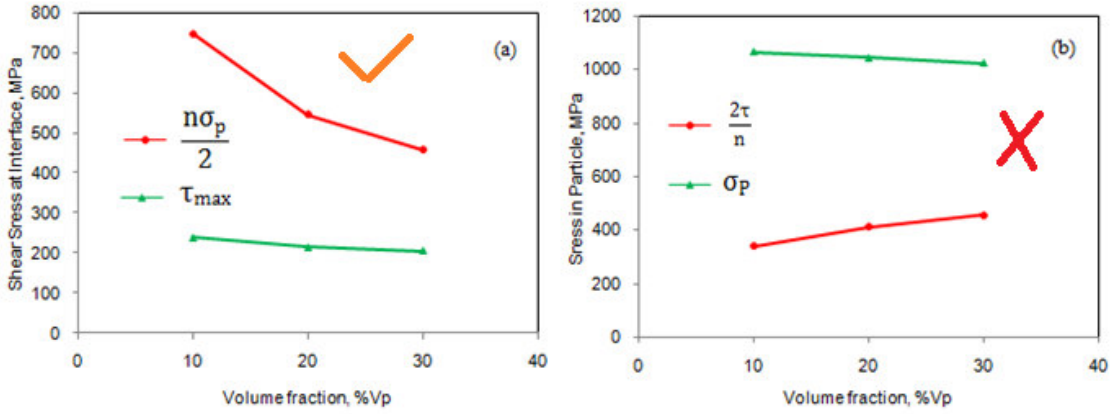

Figure 3: Fracture criteria of: (a) interface debonding and (b) particulate fracture.

The strain energy density decreased at the interface with an increase in the volume fraction of ZrC (figure 4). Also, the strain energy density of ZrC decreased in the composites. This characterizes the debonding affinity at the interface between AA8090alloy matrix and ZrC nanoparticulates. The normal and tangential tractions are plotted in figure 5a. Because of symmetry considerations, the variations of the interface stresses with circumferential location are plotted only for the range $0^o \leq \theta \leq 90^o$. For AA8090/30%ZrC composites, the normal tractions are lower than that for AA8090/10%ZrC and AA8090/20%ZrC composites. The interface debonding occurred between $0^o \leq \theta \leq 65^o$. The normal and tangential displacements are also plotted in figure 5b. The normal and tangential displacements are higher for AA8090/10%ZrC composites than those for AA8090/20%ZrC and AA8090/30%ZrC composites. For AA8090/10%ZrC, the jump in normal and tangential displacements is due to high volume fraction of AA8090 alloy matrix.

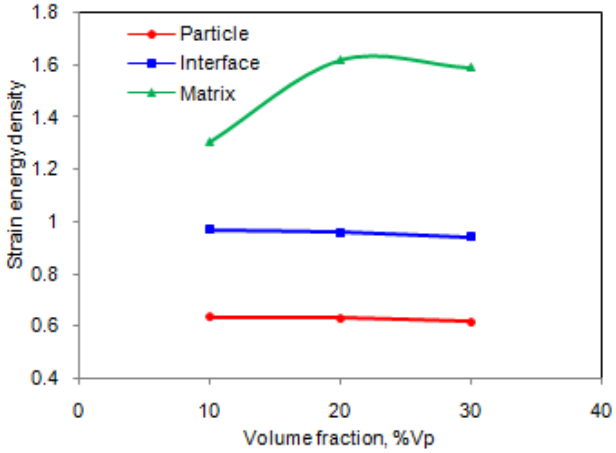

Figure 4: Effect of volume fraction on strain energy density.

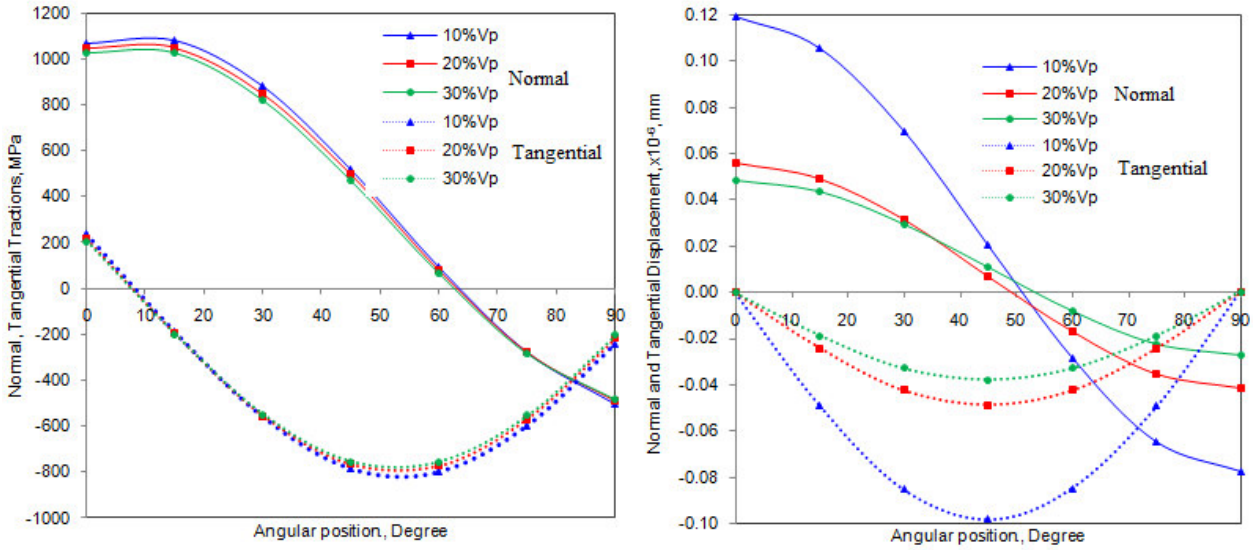

Figure 5: Normal and tangential: (a) tractions and (b) displacements.

As the raster images (figure 6) obtained from finite element analysis, the interface debonding is highest in AA8090/30%ZrC composites. On account of interface debonding the strain densities decreased with increase of ZrC volume fraction in the composite.

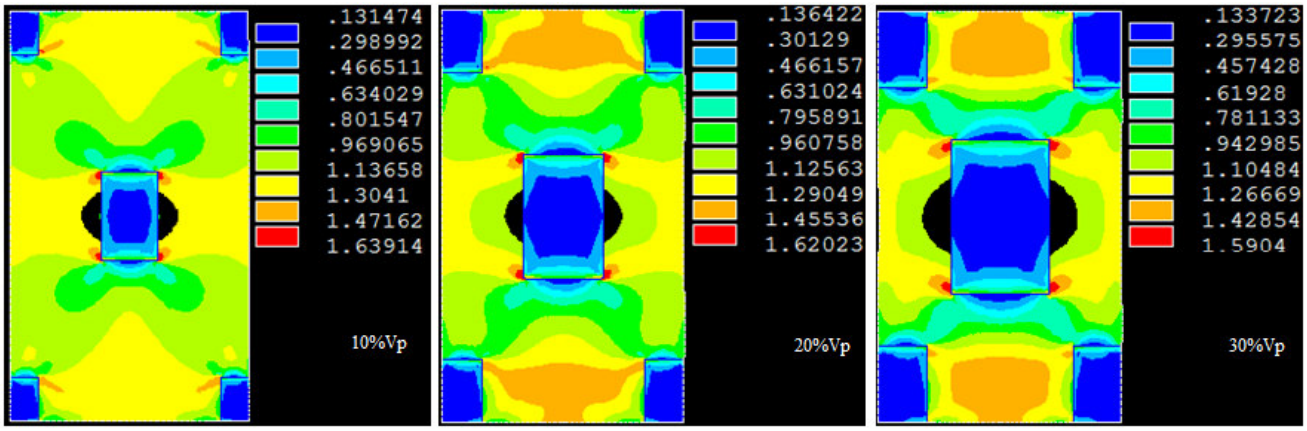

Figure 6: Strain energy densities of cohesive zones obtained from finite element analysis for debonding.

4. CONCLUSION

The interface debonding occurred in the composites containing 10%, 20% and 30% volume fractions ZrC. The interface debonding increased with an increase of volume fractions of ZrC in the composites. The strain energy density decreased with an increase of interfacial debonding in AA8090/ZrC composites.

REFERENCES

1. H. L. Cox, The elasticity and strength of paper and other fibrous materials, British Journal of applied Physics, 3, 1952, pp. 72-79.
2. M. R. Piggot, Load bearing fiber composites, Pergamon Press, New York, 1980.
3. C.W. Nan and D.R. Clarke, The influence of particle size and particle fracture on the elastic/plastic deformation of of metal matrix composite, Acta Materilia, 44, 1996, pp. 3801-3811.
4. A. Chennakesava Reddy, Assessment of Debonding and Particulate Fracture Occurrences in Circular Silicon Nitride Particulate/AA5050 Alloy Metal Matrix Composites , National Conference on Materials and Manufacturing Processes, Hyderabad, India, 27-28 February1998, pp.104-109.
5. B. Kotiveera Chari and A. Chennakesava Reddy, Numerical Simulation of Particulate Fracture in Round Silicon Nitride Particulate/AA6061 Alloy Metal Matrix Composites, National Conference on Materials and Manufacturing Processes, Hyderabad, India, 27-28 February 1998, pp. 110-114.
6. H. B. Niranjan and A. Chennakesava Reddy, Effect of Elastic Moduli Mismatch on Particulate Fracture in AA7020/Silicon Nitride Particulate Metal Matrix Composites , National Conference on Materials and Manufacturing Processes, Hyderabad, India, 27-28 February, 115-118, 1998
7. P. Martin Jebaraj and A. Chennakesava Reddy, Cohesive Zone Modelling for Interface Debonding in AA8090/Silicon Nitride Nanoparticulate Metal Matrix Composites, National Conference on Materials and Manufacturing Processes, Hyderabad, India, 27-28 February 1998, pp. 119-122.
8. P. Martin Jebaraj and A. Chennakesava Reddy, Plane Strain Finite Element Modeling for Interface Debonding in AA1100/Silicon Oxide Nanoparticulate Metal Matrix Composites, National Conference on Materials and Manufacturing Processes, Hyderabad, India, 27-28 February 1998, pp. 123-126.
9. A. Chennakesava Reddy, Local Stress Differential for Particulate Fracture in AA2024/Titanium Carbide Nanoparticulate Metal Matrix Composites, National Conference on Materials and Manufacturing Processes, Hyderabad, India, 27-28 February 1998, pp. 127-131.
10. B. Kotiveera Chari and A. Chennakesava Reddy, Interface Debonding and Particulate Facture based on Strain Energy Density in AA3003/MgO Nanoparticulate Metal Matrix Composites, National Conference on Materials and Manufacturing Processes, Hyderabad, India, 27-28 February 1998, pp. 132-136.
11. H. B. Niranjan and A. Chennakesava Reddy, Numerical and Analytical Prediction of Interface Debonding in AA4015/Boron Nitride Nanoparticulate Metal Matrix Composites , National Conference on Materials and Manufacturing Processes, Hyderabad, India, 27-28 February 1998, pp. 137-140.
12. S. Sundara Rajan and A. Chennakesava Reddy, Effect of Particulate Volume Fraction on Particulate Cracking in AA5050/Zirconium Oxide Nanoparticulate Metal Matrix Composites , National Conference on Materials and Manufacturing Processes, Hyderabad, India, 27-28 February 1998, pp. 156-159.
13. S. Sundara Rajan and A. Chennakesava Reddy, Cohesive Zone Analysis for Interface Debonding in AA6061/Titanium Nitride Nanoparticulate Metal Matrix Composites , National Conference on Materials and Manufacturing Processes, Hyderabad, India, 27-28 February 1998, pp. 160-164.
14. A. Chennakesava Reddy, Effect of Particle Loading on Microealstic Behavior and interfacial Tractions of Boron Carbide/AA4015 Alloy Metal Matrix Composites, 1st International Conference on Composite Materials and Characterization, Bangalore, 14-15 march 1997, pp. 176-179.7
15. A. Chennakesava Reddy, Reckoning of Micro-stresses and interfacial Tractions in Titanium Boride/AA2024 Alloy Metal Matrix Composites, 1st International Conference on Composite Materials and Characterization, Bangalore, 14-15 march 1997, pp. 195-197.
16. A. Chennakesava Reddy, Interfacial Debonding Analysis in Terms of Interfacial Tractions for Titanium Boride/AA3003 Alloy Metal Matrix Composites, 1st National Conference on Modern Materials and Manufacturing , Pune, India, 19-20 December 1997, pp. 124-127.
17. A. Chennakesava Reddy, Evaluation of Debonding and Dislocation Occurrences in Rhombus Silicon Nitride Particulate/AA4015 Alloy Metal Matrix Composites, 1st National Conference on Modern Materials and Manufacturing , Pune, India, 19-20 December 1997, pp. 278-282.